Journal of the European Ceramic Society **12** (1993) 257–265

Influence of the Size of the Alkali Ion on the Thermal Expansion of Alkali-Doped Cordierites: A Powder Neutron Diffraction Study

P. Thomas, D. Mercurio, I. Gouby & B. Frit*

Laboratoire de Matériaux Céramiques et Traitements de Surface, URA CNRS No. 320, Faculté des Sciences, 123 Avenue Albert-Thomas, 87060 Limoges, Cedex, France

(Received 18 February 1993; revised version received 20 April 1993; accepted 29 April 1993)

Abstract

The crystal structure of hexagonal cordierite with the formula $Cs_{0.5}Mg_2Al_{4.5}Si_{4.5}O_{18}$ *has been determined at 20, 275, 550 and 825°C by powder neutron diffraction. The mechanism of thermal expansion has been analysed and compared to that of its potassium homologue. The substitution of Cs for K results logically in an increase of the unit cell volume but in a decrease of the distortion and of the volume of the* $T(1)O_4$ *tetrahedra, and therefore in an opposite response of the tetrahedral network to the thermal expansion of the* MgO_6 *octahedra. As a consequence, the compensation of the increase in the* a*-parameter by a decrease in the* c*-parameter, observed for pure and K-doped cordierites, is no longer observed with the* $Cs_{0.5}$*-cordierite.*

Die Kristallstruktur eines hexagonalen Cordierits $Cs_{0.5}Mg_2Al_{4.5}Si_{4.5}O_{18}$ *wurde bei 20, 275, 550 und 825°C durch Neutronendiffraktion an einem Puder bestimmt. Der Mechanismus der Wärmedehnung wurde analysiert und mit dem des entsprechenden Kalium-Cordierits verglichen. Mit der Substituierung von Kalium durch Zäsium erhöht sich das Volumen einer Einheitszelle, aber die Verdrillung und das Volumen des Tetraeders* $T(1)O_4$ *werden geringer. Die Antwort des Tetraedernetzes auf die Ausdehnung der* MgO_6*-Oktaeder ist folglich entgegengesetzt zu der für rein hexagonales und mit Kalium dotiertem Cordierit. Somit wurde ein Ausgleich für das Anwachsen des Parameters* a *durch Verminderung des Parameters* c *mit Zäsium-Cordierit nicht mehr beobachtet.*

La structure cristalline de la cordiérite hexagonale $Cs_{0.5}Mg_2Al_{4.5}Si_{4.5}O_{18}$ *a été déterminée à 20, 275, 550 et 825°C par diffraction neutronique sur échantillon polycristallin. Le mécanisme de dilatation thermique a été analysé et comparé à celui de son homologue au potassium. La substitution du potassium par le césium provoque une augmentation logique du volume de la maille cristalline mais par contre une diminution de la distorsion et du volume des tétraèdres* $T(1)O_4$ *et par conséquent une réponse du réseau tétraédrique à la dilatation des octaèdres* MgO_6 *totalement opposée à celle observée pour la cordiérite hexagonale pure et pour les cordiérites dopées au potassium. La compensation de la croissance du paramètre* a *par la décroissance du paramètre* c *n'est donc plus observée avec la cordiérite au césium.*

1 Introduction

Magnesium cordierite, $MgAl_4Si_5O_{18}$, exists in two stable structural forms: the high temperature disordered hexagonal form (space group *P6/mcc*) isostructural with beryl, stable between 1450°C and its melting point (1460°C), and the low-temperature ordered orthorhombic form (space group *Cccm*) stable below 1450°C.[1–3] The hexagonal form can also be formed at lower temperatures by devitrifying a glass of cordierite composition at temperatures near 1000°C.[4] Its transformation to the orthorhombic form is very slow below 1100°C; after 200 h at this temperature, the structure is still hexagonal.[5] Because of their dielectric characteristics and their low thermal expansion coefficients, cordierite-based ceramics have numerous applications as thermal shock resistant refractories and substrates for electronic devices.

Therefore, elucidating the origin of their low thermal expansion is of practical as well as fundamental importance and several structural studies have already been devoted to both polymorphs, on

* To whom correspondence should be addressed.

Journal of the European Ceramic Society 0955-2219/93/$6.00

natural or synthetic cordierites, either pure or doped.[6-28]

For their part the present authors have shown that: (i) alkali addition stabilizes the hexagonal form whose thermal expansion is systematically lower than that of the orthorhombic form; (ii) insertion of 0·5 K atom per formula unit in the hexagonal form considerably improves the thermal properties, since the thermal expansion coefficient α, between 20 and 825°C, decreases from ≈ 2 to $0{\cdot}4 \times 10^{-6}\,K^{-1}$.[23-27]

Recently, a powder neutron diffraction study of the thermal expansion of this $K_{0{\cdot}5}Mg_2Al_{4{\cdot}5}Si_{4{\cdot}5}O_{18}$ ceramic, allowed the authors to show that its thermal behaviour is essentially of the same nature as for pure hexagonal cordierite, but is very dependent on the presence of potassium atoms within the channels of the structure.[25] In order to better understand the structural role played by alkali atoms, the authors decided to undertake the same kind of structural study on a $Cs_{0{\cdot}5}Mg_2Al_{4{\cdot}5}Si_{4{\cdot}5}O_{18}$ hexagonal cordierite, containing the same proportion of a more voluminous alkali ion, i.e. cesium.

2 Experimental

The Cs-cordierite was prepared with the same experimental procedure as the corresponding K-cordierite. Weighed quantities of high purity $SiO_{2-x}H_2O$, Al_2O_3, MgO and Cs_2CO_3, corresponding to the $Cs_{0{\cdot}5}Mg_2Al_{4{\cdot}5}Si_{4{\cdot}5}O_{18}$ composition, were ball-milled for 2 h in plastic bottles, cold-pressed at 50 MPa and then sintered at 1300°C for 2 h under air atmosphere. The large bars obtained were then melted in an oxyhydric flame and quenched in cold water. The glass pieces thus formed were ball-milled for 2 h and uniaxially pressed into a cylindrical bar (≈ 9 mm in diameter and 65 mm long) necessary for neutron diffraction experiments. The sample was heated again for 2 h at 1000°C and 2 h at 1160°C. Such a process ensures complete crystallization and gives apparently pure hexagonal cordierite, i.e. no splitting or broadening of the (211) hexagonal peak on X-ray diagrams (Guinier–Hagg camera and D-5000 Siemens diffractometer; CuK_α).

The neutron diffraction experiments were performed at the Centre d'Etudes Nucléaires (CEN) in Grenoble, between 20 and 825°C, using the time-of-flight powder neutron diffraction technique previously used for the K-bearing cordierite. This method, described elsewhere in detail,[29] presents several advantages, mainly:

(i) The whole spectrum is recorded as a function of time at a fixed scattering angle ($2\theta = 90°$).
(ii) The resolution is excellent over a larger range of d-spacings than for conventional diffraction techniques.
(iii) A large number of reflections are registered (141 for the present study) with a constant and very good resolution ($\approx 3 \times 10^{-5}$ nm).

The diffraction patterns recorded as for K samples, at 20, 275, 550 and 825°C, were fitted to calculated ones, using a full profile analysis programme (Rietveld method modified for time-of-

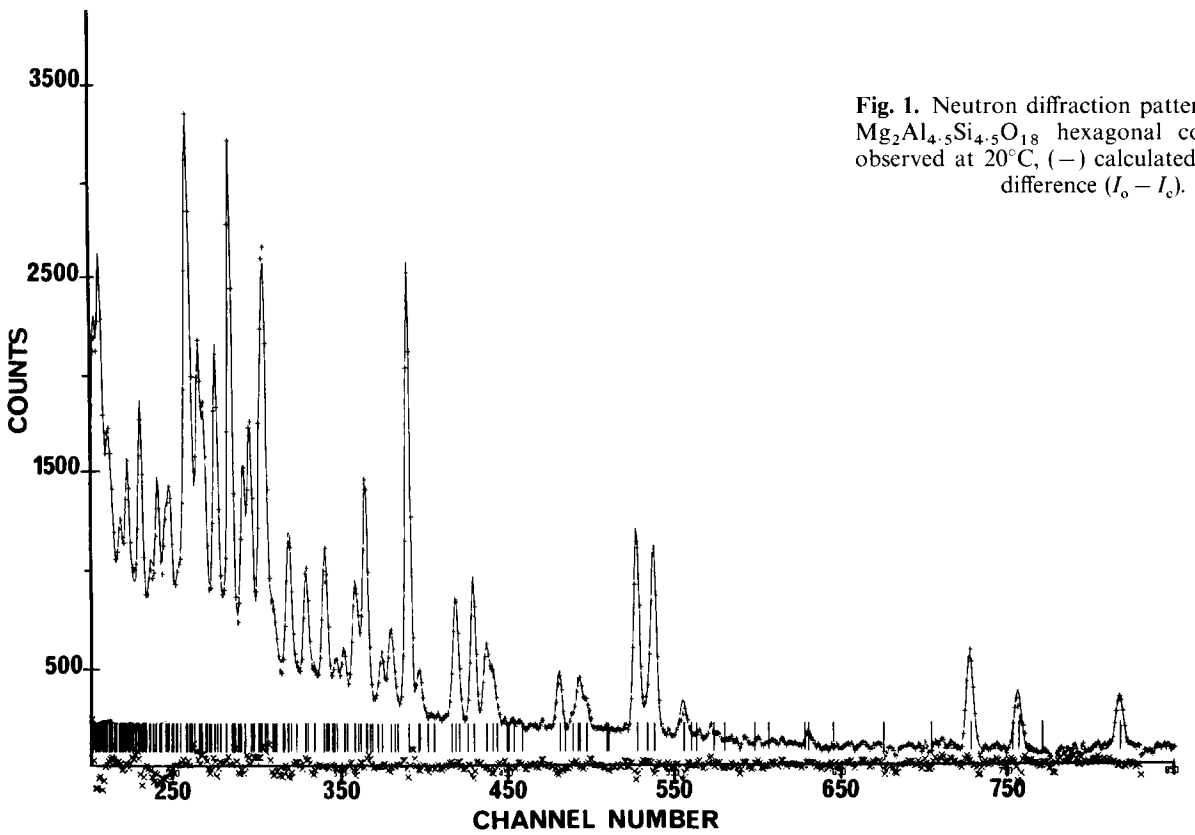

Fig. 1. Neutron diffraction patterns for $Cs_{0{\cdot}5}Mg_2Al_{4{\cdot}5}Si_{4{\cdot}5}O_{18}$ hexagonal cordierite (+) observed at 20°C, (−) calculated and (×) the difference ($I_o - I_c$).

flight neutron diffraction data),[30] in order to minimize the profile discrepancy factor

$$R_p = \frac{\sum_i |y_i - y(\lambda_i)|}{\sum_i y_i}$$

where y_i is the observed value at the ith channel, and $y(\lambda_i)$ is the calculated value of the fitting function at the same ith channel. Calculations were carried out in the *P6/mcc* group, using the structural data of the study on $K_{0.5}Mg_2Al_{4.5}Si_{4.5}O_{18}$ as starting values and the following coherent scattering lengths: 0·542, 0·5375, 0·4149, 0·3449 and 0·5805 ($\times 10^{-5}$ nm) for cesium, magnesium, silicon, aluminium and oxygen, respectively. In each case, 16 variables were refined simultaneously, including: lattice parameters, scale factor, atomic coordinates not fixed by the space group, isotropic thermal coefficients, and occupancies (Si/Si + Al) of the tetrahedral sites (T(1) and T(2) constrained to respect the chemical compositions. Based on the results of an X-ray fluorescence analysis the occupancy factor was fixed to $\frac{1}{4}$ for cesium. The final refinements converged for each temperature to R_p values less than 5%.

The neutron diffraction pattern at room temperature, illustrating the fit profile obtained, is shown in Fig. 1.

3 Results and Discussion

The refined structural parameters are listed in Table 1 and the main interatomic distances and bond angles are given in Table 2.

3.1 Structure at room temperature

The results at room temperature are in good agreement with all previous results concerning K- and Cs-bearing hexagonal cordierites.[11,13,20,27]

A projection of the structure along Oz is shown in Fig. 2. The arrangement of the polyhedra, which is typical of the hexagonal pure cordierite framework, is depicted in Fig. 3. It consists of six-membered rings of $T(2)O_4$ tetrahedra, centred at the origin, stacked one above the other and successively rotated approximately 30° relative to each other (Fig. 3(a)). These rings are connected vertically and horizontally by $T(1)O_4$ tetrahedra and MgO_6 octahedra, which, by sharing edges, form a two-dimensional network of large overlapping 12-membered rings parallel to xOy. Figure 3(b) shows the alternate sequence along Oz of the $T(2)O_4$ (at $z = 0, \frac{1}{2}$) and $[T(1)O_4–MgO_6]$ (at $z \approx \frac{1}{4}, \frac{3}{4}$) sheets, the heights of which are respectively labelled $H_{T(2)}$ and H_M.

The stacking of the six-membered rings produces large channels, parallel to the *c*-axis, in which the Cs

Table 1. Final structural parameters for $Cs_{0.5}Mg_2Al_{4.5}Si_{4.5}O_{18}$ cordierite (standard deviation in parentheses)

		20° C	275° C	550° C	825° C
Mg (4c)	x	$\frac{1}{3}$	$\frac{1}{3}$	$\frac{1}{3}$	$\frac{1}{3}$
	y	$\frac{2}{3}$	$\frac{2}{3}$	$\frac{2}{3}$	$\frac{2}{3}$
	z	$\frac{1}{4}$	$\frac{1}{4}$	$\frac{1}{4}$	$\frac{1}{4}$
	B ($\times 10^{-2}$ nm^2)	0·02 (9)	0·34 (7)	0·71 (11)	0·94 (12)
T(1) (6f)	x	$\frac{1}{2}$	$\frac{1}{2}$	$\frac{1}{2}$	$\frac{1}{2}$
	y	0	0	0	0
	z	$\frac{1}{4}$	$\frac{1}{4}$	$\frac{1}{4}$	$\frac{1}{4}$
	τ (Si)	0·50	0·52	0·51	0·52
	B ($\times 10^{-2}$ nm^2)	0·34 (8)	0·46 (7)	0·65 (10)	0·91 (10)
T(2) (12l)	x	0·372 8 (3)	0·372 4 (3)	0·371 5 (4)	0·371 1 (3)
	y	0·267 1 (4)	0·267 7 (3)	0·268 5 (4)	0·268 0 (4)
	z	0	0	0	0
	τ (Si)	0·50 (2)	0·48 (2)	0·49 (2)	0·48 (2)
	B ($\times 10^{-2}$ nm^2)	0·12 (5)	0·27 (5)	0·16 (6)	0·36 (7)
O(1) (24m)	x	0·486 1 (1)	0·485 8 (1)	0·485 2 (2)	0·485 2 (2)
	y	0·350 7 (2)	0·350 8 (1)	0·350 6 (2)	0·350 7 (2)
	z	0·143 9 (2)	0·143 7 (1)	0·143 2 (2)	0·143 7 (2)
	B ($\times 10^{-2}$ nm^2)	0·48 (3)	0·81 (3)	0·25 (4)	1·54 (4)
O(2) (12l)	x	0·228 3 (3)	0·227 6 (2)	0·228 1 (3)	0·226 7 (4)
	y	0·303 9 (3)	0·304 0 (3)	0·304 7 (4)	0·304 4 (4)
	z	0	0	0	0
	B ($\times 10^{-2}$ nm^2)	1·55 (4)	2·07 (4)	2·57 (5)	2·92 (6)
Cs (4e)	x	0	0	0	0
	y	0	0	0	0
	z	0·233 2 (44)	0·249 4 (70)	0·249 8 (51)	0·249 5 (80)
	B ($\times 10^{-2}$ nm^2)	1·42 (50)	3·33 (51)	3·08 (70)	4·22 (42)
a (nm)		0·980 49 (2)	0·980 87 (2)	0·981 73 (2)	0·982 53 (2)
c (nm)		0·938 42 (3)	0·938 28 (3)	0·938 57 (4)	0·939 12 (4)
v (nm^3)		0·781 29	0·781 78	0·783 40	0·785 13
R_p (%)		4·1	4·0	4·0	4·5

Table 2. Main interatomic distances (nm) and bond angles (°) for $Cs_{0.5}Mg_2Al_{4.5}Si_{4.5}O_{18}$ cordierite (standard deviation in parentheses)

	20°C	*275°C*	*550°C*	*825°C*
T(2)–T(2)^1	0·326 3 (5)	0·326 3 (4)	0·326 1 (5)	0·326 0 (5)
T(2)–T(2)^2	0·495 2 (5)	0·495 6 (4)	0·496 6 (5)	0·496 7 (5)
T(2)–T(1)	0·307 1 (2)	0·306 7 (2)	0·306 5 (3)	0·307 0 (3)
T(2)–Mg	0·351 6 (2)	0·352 0 (2)	0·353 1 (3)	0·353 4 (3)
T(1)–Mg	0·283 1	0·283 2	0·283 5	0·283 7
T(2)–Cs	0·392 9 (10)	0·401 5 (10)	0·401 7 (10)	0·402 0 (10)
T(1)–Cs	0·490 5 (10)	0·490 4 (10)	0·490 9 (10)	0·491 3 (10)
Cs–O(2) (×6)	0·367 3 (10)	0·357 0 (10)	0·357 2 (10)	0·357 0 (10)
Cs–O(2)^3 (×6)	0·346 5 (10)	0·356 3 (10)	0·357 5 (10)	0·357 6 (10)
⟨Cs–O⟩	0·356 9	0·356 6	0·357 3	0·357 3
Cs–O(1) (×6)	0·441 4 (10)	0·437 7 (10)	0·437 6 (10)	0·437 7 (10)
Cs–O(1) (×6)	0·434 2 (10)	0·437 4 (10)	0·437 6 (10)	0·437 9 (10)
T(1)–O(1) (×4)	0·171 9 (2)	0·171 8 (1)	0·172 2 (2)	0·171 9 (2)
O(1)–O(1)^1 (×2)	0·304 2 (3)	0·304 0 (2)	0·304 3 (4)	0·303 7 (4)
O(1)–O(1)^3 (×2)	0·255 5 (3)	0·255 9 (2)	0·257 3 (4)	0·256 6 (4)
O(1)–O(1)^2 (×2)	0·280 1 (3)	0·279 8 (2)	0·279 9 (4)	0·280 0 (4)
⟨O–O⟩ (T(1))	0·279 9	0·279 9	0·280 5	0·280 1
T(2)–O(1) (×2)	0·167 9 (3)	0·167 7 (2)	0·167 4 (3)	0·168 1 (3)
T(2)–O(2)	0·162 8 (3)	0·162 8 (3)	0·161 5 (3)	0·162 7 (4)
T(2)–O(2)^1	0·164 7 (3)	0·164 7 (3)	0·165 6 (3)	0·164 3 (4)
⟨T(2)–O⟩	0·165 8	0·165 7	0·165 5	0·165 8
O(2)–O(2)^1	0·268 7 (4)	0·268 7 (3)	0·269 5 (5)	0·269 2 (5)
O(1)–O(2) (×2)	0·269 5 (3)	0·269 8 (2)	0·269 1 (3)	0·270 6 (3)
O(1)–O(2)^1 (×2)	0·273 3 (3)	0·272 8 (2)	0·272 8 (2)	0·272 3 (3)
O(1)–O(1)	0·270 1 (3)	0·269 7 (2)	0·268 8 (4)	0·269 9 (4)
⟨O–O⟩ (T(2))	0·270 7	0·270 6	0·270 2	0·270 8
Mg–O(1) (×6)	0·211 1 (2)	0·211 6 (1)	0·212 4 (2)	0·212 4 (2)
O(1)^1–O(1)^4 (×3)	0·290 2 (3)	0·290 9 (2)	0·291 8 (4)	0·291 5 (4)
O(1)^1–O(1)^2 (×3)	0·255 5 (3)	0·255 9 (2)	0·257 3 (4)	0·256 6 (4)
O(1)^2–O(1)^4 (×6)	0·322 4 (3)	0·323 1 (2)	0·324 2 (4)	0·324 6 (4)
⟨O–O⟩ (Mg)	0·297 6	0·298 2	0·299 4	0·299 3
O(1)^1–T(1)–O(1)^2 (×2)	96·02	96·26	96·68	96·54
O(1)^1–T(1)–O(1)^3 (×2)	109·19	109·03	108·79	109·01
O(1)^1–T(1)–O(1) (×2)	124·51	124·40	124·17	124·08
⟨O–T(1)–O⟩	109·91	109·90	109·88	109·88
O(2)^1–T(2)–O(2)	110·27	110·26	110·93	110·77
O(2)^1–T(2)–O(1) (×2)	110·53	110·31	109·70	109·88
O(2)–T(2)–O(1) (×2)	109·18	109·44	109·80	109·74
O(1)–T(2)–O(1)	107·08	107·01	106·81	106·76
⟨O–T(2)–O⟩	109·46	109·46	109·46	109·46
O(1)–Mg–O(1)^3 (×3)	74·45	74·41	74·54	74·34
O(1)–Mg–O(1)^5 (×3)	86·83	86·84	86·79	86·69
O(1)^3–Mg–O(1)^5 (×6)	99·56	99·58	99·53	99·69
⟨O–Mg–O⟩	90·10	90·10	90·10	90·10
T(2)–O(2)–T(2)^1	171·97	171·94	172·06	172·00
T(2)–O(1)–T(1)	129·28	129·22	129·02	129·04
T(2)–O–T(2)^{2a}	28·07	28·36	28·85	28·78

[a] The value given is not the real value of the T(2)–O–T(2)^2 angle but the value of its projection onto the xOy plane.

atoms are located, statistically distributed among the 4*e* position (0, 0, *z*).

Ideal [T(1)O_4–MgO_6] rings (i.e. built up with regular tetrahedra and octahedra) would not be large enough to fit around the six-membered T(2)O_4 rings. As observed with pure cordierite[11] and $K_{0.5}Mg_2Al_{4.5}Si_{4.5}O_{18}$[25] they are therefore severely distorted: the T(1)O_4 tetrahedra are elongated along one of their $\bar{4}$ axes parallel to the xOy plane, and the MgO_6 octahedra are stretched isotropically along the same plane (see Table 3).

As previously shown[11,20,25] and as indicated by the values reported in Tables 3 and 4, if the alkali insertion does not induce any important regularization of the polyhedra, on the other hand it leads logically to an increase of the lattice parameters, mainly as a result of the expansion of the six-membered T(2)O_4 rings, which become richer in aluminium.[28]

More particularly, the substitution of Cs for K in the channels results in

(1) a logical increase of the unit cell volume,
(2) a change in the *z*-coordinate of the Cs atoms relative to *K* ($z \approx 0{\cdot}19$ for K and $z \approx 0{\cdot}23$ for Cs).

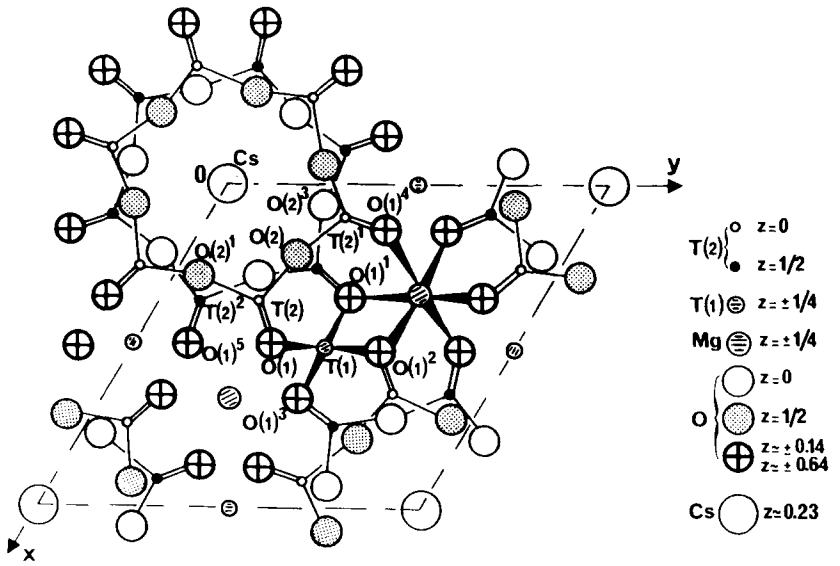

Fig. 2. Projection along the c-axis of the $Cs_{0.5}Mg_2Al_{4.5}Si_{4.5}O_{18}$ cordierite structure at room temperature.

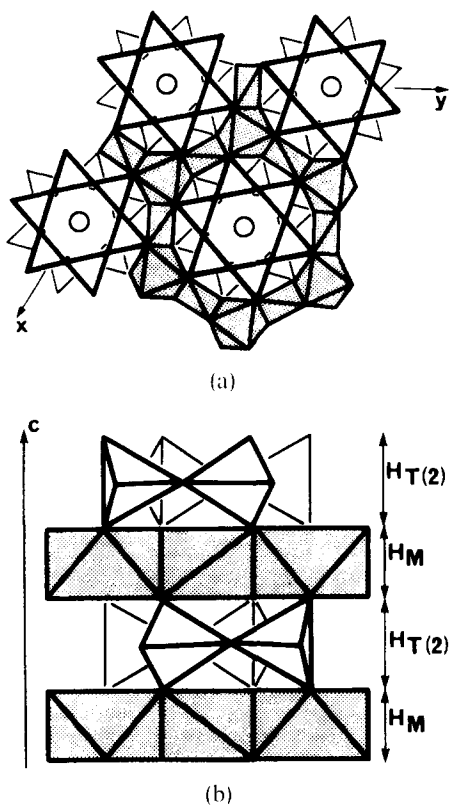

Fig. 3. Schematic representation of the hexagonal cordierite structure viewed (a) along the c-axis, (b) normal to the c-axis.

As a consequence, whereas the K atoms are tightly bound to six nearest O(2) atoms of the same closest ring ($K–O(2)^1 \approx 0{\cdot}32$ nm) and more loosely bound to six O(2) atoms of the next ring ($K–O(2)^3 \approx 0{\cdot}40$ nm), the Cs atoms, located almost midway between two successive rings, are nearly symmetrically surrounded by twelve oxygen atoms ($6Cs–O(2) \approx 0{\cdot}37$ nm and $6Cs–O(2) \approx 0{\cdot}35$ nm).

In fact, O(1) and O(2) atoms are more symmetrically and more strongly bound to Cs than to K atoms, which allows (see Tables 2–4):

(1) A lower distortion of the $T(1)O_4$ and especially $T(2)O_4$ tetrahedra.

(2) A lower thickness (H_M) of the $[T(1)O_4–MgO_6]$ sheets and especially of the $T(1)O_4$ tetrahedra, which are therefore less voluminous and more regular. It is this decrease of H_M which explains the small decrease of the c-parameter when Cs is substituted for K.

It will be seen later, that such differences, at first sight not very significant, can however induce important changes in the thermal behaviour of alkali-bearing cordierites.

3.2 Thermal behaviour

The thermal changes of the lattice parameters a and c and their effects on the global volume expansion are compared with those of the homologous K-bearing cordierite[25] and of the pure cordierite[11] in Figs 4 and 5. It can be seen that the compensation of the a-parameter increase by the c-parameter decrease, observed for pure and K-bearing cordierites, and whose net result is, especially with the $K_{0.5}$-cordierite, a very low mean thermal expansion coefficient $\bar{\alpha}$, is no longer observed with the $Cs_{0.5}$-cordierite. This difference can be understood by a comparative detailed structural analysis of the thermal behaviour of these three phases, on the basis of the values given in Tables 2–4 and of the changes shown in Figs 6 and 7.

As in pure and K-bearing cordierites, the thermal expansions of the $T(1)O_4$ and $T(2)O_4$ tetrahedra are small compared with the expansion of the MgO_6 octahedron (see values in Table 2) and, therefore, the structural changes with temperature mainly depend on the way the tetrahedral network adapts itself to the octahedral expansion.

Table 3. Distortion indices σ^a of the $T(1)O_4$, $T(2)O_4$ and MgO_6 polyhedra, at various temperatures in (a) K-[25] and Cs-bearing cordierites and (b) pure cordierite[11]

	σ 20°C		σ 275°C		σ 550°C		σ 825°C	
	$K_{0.5}$	$Cs_{0.5}$	$K_{0.5}$	$Cs_{0.5}$	$K_{0.5}$	$Cs_{0.5}$	$K_{0.5}$	$Cs_{0.5}$
T(1)	13·05	12·76	12·46	12·61	12·54	12·33	12·04	12·34
T(2)	1·96	1·32	0·50	1·27	0·78	1·38	0·52	1·38
Mg	10·48	10·89	11·05	10·91	11·07	10·84	11·25	11·00

(a)

	σ 22°C	σ 228°C	σ 500°C	σ 750°C
T(1)	12·33	11·17	11·98	11·71
T(2)	1·75	1·69	1·87	2·04
Mg	10·79	10·92	10·99	11·23

(b)

[a] σ values were calculated from the expression:[31]

$$\sigma^2 = \sum_{i=1}^{m} (\theta_i - \theta_0)^2/m - 1$$

where θ_0 is the undistorted bond angle subtended by an edge of the polyhedron at the centre atom (e.g. 109·47° for a tetrahedron and 90° for an octahedron). When there is no distortion $\sigma = 0$.

Table 4. Comparison of the unit cell parameters (nm) and volume (nm^3) and of the main distances (nm) and angles (°) in pure cordierite, K- and Cs-bearing cordierites at room temperature

	Pure hexagonal cordierite[11]	$K_{0.5}Mg_2Al_{4.5}Si_{4.5}O_{18}$[25]	$Cs_{0.5}Mg_2Al_{4.5}Si_{4.5}O_{18}$ *(this work)*
a	0·977 28	0·979 10	0·980 49
c	0·934 89	0·939 69	0·938 42
v	0·773 27	0·780 13	0·781 29
⟨T(2)–O⟩	0·164 8	0·165 8	0·165 8
⟨O–O⟩T(2)	0·268 5	0·270 7	0·270 7
O(1)–O(1) = $H_{T(2)}$	0·269 1	0·270 4	0·270 1
⟨T(1)–O⟩	0·172 1	0·173 1	0·171 9
O(1)–O(1)^2	0·281 4	0·283 0	0·280 1
O(1)–O(1)^3	0·256 3	0·256 2	0·255 5
O(1)–O(1)^1	0·303 6	0·306 5	0·304 2
<O–O>T(1)	0·280 4	0·281 9	0·279 9
$H_{T(1)}$	0·198 3	0·199 4	0·199 1
⟨Mg–O⟩	0·210 6	0·209 8	0·211 1
⟨O–O⟩Mg	0·297 0	0·295 9	0·297 6
⟨M–O(2)⟩ (×12)	—	0·358	0·357
⟨M–O(1)⟩ (×12) (M = K, Cs)	—	0·440	0·438
T(2)–O–T(2)^2	27·77	26·52	28·07

As previously shown for pure and $K_{0.5}$-cordierite, two stages can still be distinguished, but the changes in the tetrahedral network are completely opposite.

3.2.1 First stage: 20 to ≈500°C

With increasing temperature, an anisotropic expansion of the MgO_6 octahedra (i.e. mainly in the *xOy* plane) is observed in pure and $K_{0.5}$-cordierite.

This is possible thanks to the regularization (flattening parallel to [110]; see Fig. 6) and to the contraction of the $T(1)O_4$ tetrahedra, and results in a flattening of the 12-membered $[T(1)O_4–MgO_6]$ sheets (decrease of H_M) and in a correlative thickening of the six-membered $T(2)O_4$ sheets (increase of $H_{T(2)}$ mainly due to vertical movements of O(1) atoms (for more details see Ref. 25)).

With the $Cs_{0.5}$-cordierite, this behaviour is no longer possible, simply because, as has already been indicated, the $T(1)O_4$ tetrahedra are much more regular and smaller. This expansion therefore occurs isotropically (i.e. expansion of all edges, including the shared O(1)–O(1)^3 edge; see Table 2) resulting in a thickening of the $[T(1)O_4–MgO_6]$ sheets (increase of H_M) and a corresponding flattening of the $T(2)O_4$ rings (decrease of $H_{T(2)}$) facilitated by the outward movement of the O(1) atoms (contrary to $K_{0.5}$-cordierite: see arrows on Fig. 6).

This phenomenon is disturbed below 200°C by the

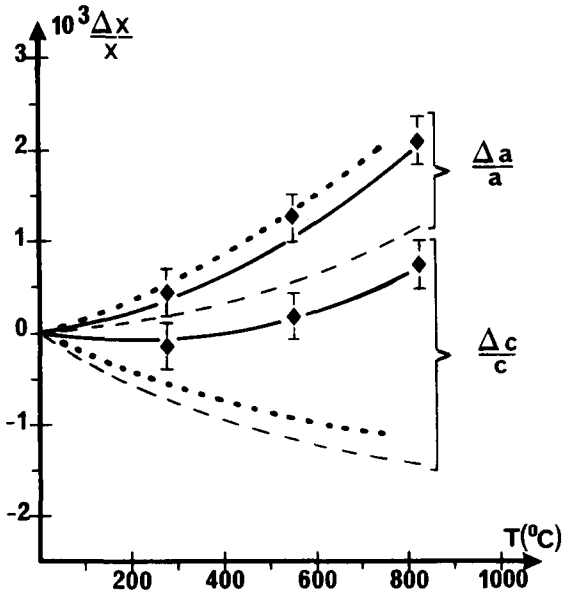

Fig. 4. Thermal evolution of the lattice parameters for (– – –) pure,[11] (– · · –) $K_{0.5}$-[25] and (———) $Cs_{0.5}$-doped cordierites.

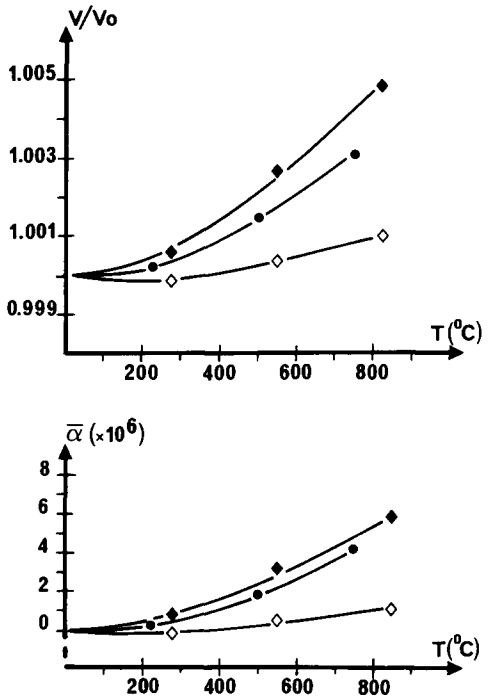

Fig. 5. Thermal expansion of (●) pure,[11] (◇) $K_{0.5}$-[25] and (◆) $Cs_{0.5}$-doped cordierites.

vertical displacement of Cs atoms within the channels (the z-coordinate changes from 0·23 to ≈ 0·25). This change favours an increase of $H_{T(2)}$ and a decrease of H_M so that a small decrease of the c-parameter is observed during the first step of heating (see curves in Fig. 4).

3.2.2 Second stage: ≈ 500 to 825°C

At higher temperatures, as observed for pure cordierite, and as probably would have been observed for $K_{0.5}$-cordierite (see hypothetical curves shown as dashed lines in Fig. 7) without the occurrence of a specific partial Al/Si ordering within the $T(1)O_4$ and $T(2)O_4$ tetrahedra (see Ref. 25), the thermal behaviour is reversed: H_M decreases and $H_{T(2)}$ increases. The MgO_6 octahedra are too large to carry on expanding isotropically without seriously weakening the Mg–O bond strength. They now expand anisotropically by elongating along the xOy plane and flattening along Oz, to the detriment of oblique edges such as the common $O(1)$–$O(1)^3$ edges which are now long enough to accommodate the corresponding contraction.

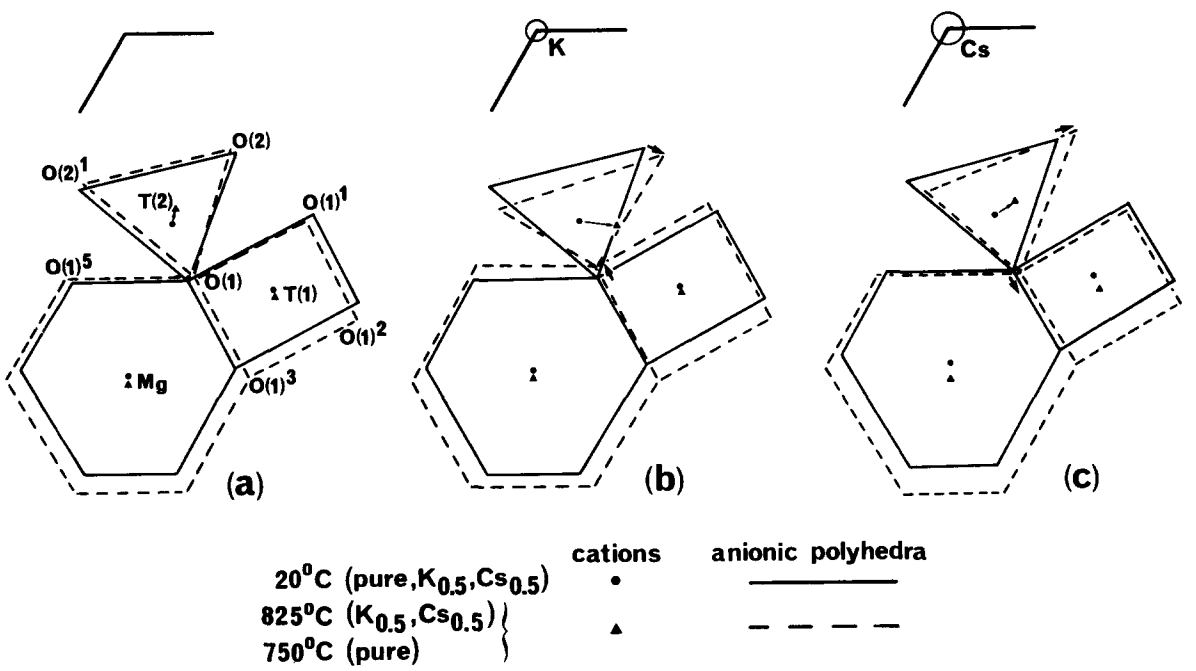

Fig. 6. Displacements with temperature (magnified 20 times) of the atoms which form the three basic polyhedra MgO_6, $T(1)O_4$ and $T(2)O_4$ for (a) pure cordierite,[11] (b) $K_{0.5}$-cordierite,[25] (c) $Cs_{0.5}$-cordierite. This representation, very useful for the comparison of the relative movements of atoms in the xOy basal plane, is not, of course, representative of their actual positions.

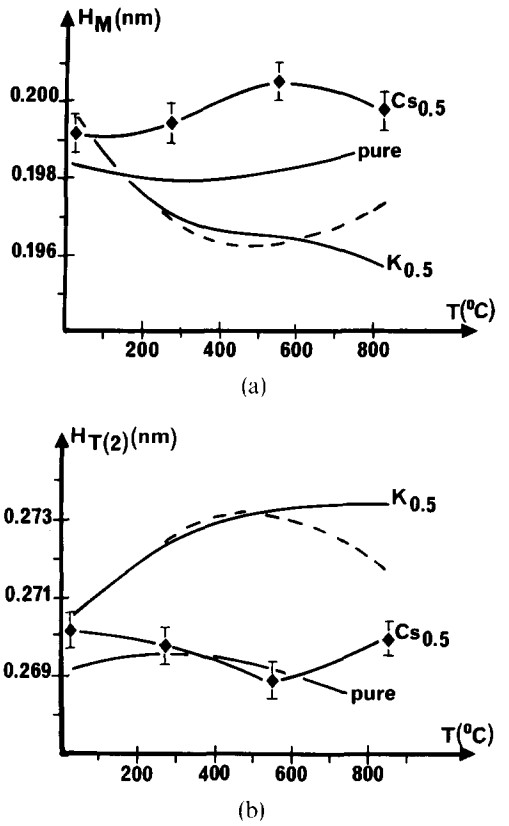

Fig. 7. Thermal evolution of the heights (a) H_M and (b) $H_{T(2)}$ of, respectively, the $[T(1)O_4$–$MgO_6]$ and $T(2)O_4$ sheets in pure, $K_{0.5}$- and $Cs_{0.5}$-cordierites.

4 Conclusion

The low thermal expansion of hexagonal cordierites is a consequence of the decrease in the *c*-parameter which compensates for the increase in the *a*-parameter with increasing temperature.

This behaviour, which results from a complex and opposite change in the thickness of the six-membered $T(2)O_4$ and the twelve-membered $[T(1)O_4$–$MgO_6]$ sheets, is still observed when potassium atoms are inserted within the hexagonal channels, because these atoms (as long as the insertion rate remains moderate, i.e. $\leq 0{\cdot}5$ atom per formula unit) are not located midway between successive six-membered $T(2)O_4$ rings ($z < 0{\cdot}25$) and so do not inhibit the contraction along O*z*. Cs atoms which are much larger immediately reach the limiting ($z = 0{\cdot}25$) position. Stronger Cs–O bonds are generated, which stiffen the aluminosilicate framework and inhibit any significant structural changes. So, in contrast to potassium, cesium insertion in hexagonal cordierite does not have a favourable effect by reducing thermal expansion.

Acknowledgements

The authors wish to thank G. Roult from CEN Grenoble for powder neutron diffraction experiments and for numerous useful discussions.

References

1. Gibbs, G. V., The polymorphism of cordierite I: the crystal structure of low cordierite. *Am. Mineral.*, **51** (1966) 1068–87.
2. Cohen, J. B., Ross, F. K. & Gibbs, G. V., An X-ray and neutron diffraction study of hydrous low cordierite. *Am. Mineral.*, **62** (1977) 67–78.
3. Meagher, E. P. & Gibbs, G. V., The polymorphism of cordierite II: the crystal structure of indialite. *Can. Mineral.*, **15** (1977) 43–9.
4. Langer, K. & Schreyer, W., Infrared and powder X-ray diffraction studies on the polymorphism of cordierite, $Mg_2(Al_4Si_5O_{18})$. *Am. Mineral.*, **54** (1969) 1442–59.
5. Putnis, A. & Bish, D. L., The mechanism and kinetics of Al, Si ordering in Mg-cordierite. *Am. Mineral.*, **68** (1983) 60–5.
6. Hochella, Jr, M. F. & Brown, Jr, G. E., Structural mechanisms of anomalous thermal expansion of cordierite-beryl and other framework silicates. *J. Am. Ceram. Soc.*, **69** (1986) 13–18.
7. Lee, J. D. & Pentecost, J. L., Properties of flux-grown cordierite single crystals. *J. Am. Ceram. Soc.*, **59** (1976) 183.
8. Milberg, M. E. & Blair, H. D., Thermal expansion of cordierite. *J. Am. Ceram. Soc.*, **60** (1977) 372–3.
9. Evans, D. L., Fischer, G. R., Geiger, J. E. & Martin, F. W., Thermal expansions and chemical modifications of cordierite. *J. Am. Ceram. Soc.*, **63** (1980) 629–34.
10. Ikawa, H., Otagiri, T., Imai, O., Suzuki, M., Urabe, K. & Udagawa, S., Crystal structures and mechanism of thermal expansion of high cordierite and its solid solutions. *J. Am. Ceram. Soc.*, **69** (1986) 492–8.
11. Predecki, P., Haas, J., Faber, Jr, J. & Hitterman, R. L., Structural aspects of the lattice thermal expansion of hexagonal cordierite. *J. Am. Ceram. Soc.*, **70** (1987) 175–82.
12. Predecki, P., Haas, J., Faber, Jr, J. & Hitterman, R. L., Lattice thermal expansion effects in pure and doped cordierite by time-of-flight neutron diffraction. *Adv. X-Ray Anal.*, **29** (1986) 173–84.
13. Haas, J., Predecki, P., Faber, Jr, J. & Hitterman, R. L., Thermal expansion behavior of pure and doped cordierite by time-of-flight neutron diffraction. *Adv. X-Ray Anal.*, **30** (1987) 395–405.
14. Armbruster, T., Crystal structure refinement, Si, Al-ordering, and twinning in 'pseudo-hexagonal' Mg-cordierite. *N. Jb. Miner. Mh.*, **6** (1985) 255–67.
15. Armbruster, T., Crystal structure refinement and thermal expansion of a Li, Na, Be-cordierite between 100 and 550 K. *Z. Kristall.*, **174** (1986) 205–17.
16. Schreyer, W., Experimental studies on cation substitutions and fluid incorporation in cordierite. *Bull. Mineral.*, **108** (1985) 273–91.
17. Wolfsdorff, P. & Schreyer, W., Synthesis of sodian cordierites in the system Na_2O–MgO–Al_2O_3–SiO_2. *N. Jb. Miner. Mh.*, **2** (1992) 80–96.
18. Daniels, P., What is the true space group of high cordierite? *Z. Kristall.*, **190** (1990) 271–6.
19. Schreyer, W., Maresch, W. V., Daniels, P. & Wolfsdorff, P., Potassic cordierites: characteristic minerals for high-temperature, very low-pressure environments. *Contrib. Mineral. Petrol.*, **105** (1990) 162–72.
20. Daniels, P., Structural effects of the incorporation of large-radius alkalis in high cordierite. *Am. Mineral.*, **77** (1992) 407–11.
21. Daniels, P. & Gies, H., NMR-spectroscopy of synthetic potassium-bearing cordierites. *Phys. Chem. Minerals*, **18** (1992) 383–8.
22. Putnis, A., Salje, E., Redfern, S. A. T., Fyfe, C. A. & Strobl, H., Structural states of Mg-cordierite I: order parameters from synchrotron X-ray and NMR data. *Phys. Chem. Minerals*, **14** (1987) 446–54.
23. Kim, Y. H., Mercurio, D., Mercurio, J. P. & Frit, B., Structural study of a K-substituted synthetic cordierite. *Mater. Res. Bull.*, **19** (1984) 209–17.

24. Mercurio, J. P., Mercurio, D., Frit, B., Kim, Y. H. & Roult, G., High temperature crystal chemistry of a low thermal expansion material: K-substituted cordierite. In *High Tech Ceramics, Material Science Monographs*,Vol. 38, Elsevier Science, Amsterdam, 1987, pp. 361–7.
25. Mercurio, D., Thomas, P., Mercurio, J. P., Frit, B., Kim, Y. H. & Roult, G., Powder neutron diffraction study of the thermal expansion of a K-substituted cordierite. *J. Mater. Sci.*, **24** (1989) 3976–83.
26. Mercurio, D., Thomas, P., Mercurio, J. P., Frit, B. & Roult, G., Thermal expansion study of alkali-substituted cordierites. In *Proceedings of the First European Ceramics, Euro Ceramics*, Vol. 2, Maastricht, 1989, pp. 72–6.
27. Thomas, P., Mercurio, D., Mercurio, J. P. & Frit, B., Powder neutron diffraction study of alkali-substituted cordierites with $M_xMg_2Al_{4+x}Si_{5-x}O_{18}$ ($M = K, Cs; 0 < x \leq 1$) formula. *Eur. J. Solid State Inorg. Chem.*, **28** (1991) 1011–20.
28. Senegas, J., Grimmer, A. R., Muller, D., Thomas, P., Mercurio, D. & Frit, B., Determination of the Al/Si distribution in synthetic $K_xMg_2Al_{4+x}Si_{5-x}O_{18}$ ($0 < x \leq 1$) cordierites by ^{29}Si and ^{27}Al MAS–NMR spectroscopy. *J. Mater. Sci.*, **26** (1991) 5053–9.
29. Roult, G. & Buevoz, J. L., A time-of-flight spectrometer for elastic neutron scattering on powdered samples. *Rev. Phys. Appl.*, **12** (1977) 581–90.
30. Rietveld, H. M., A profile refinement method for nuclear and magnetic structures. *J. Appl. Crystall.*, **2** (1969) 65–71.
31. Robinson, K., Gibbs, G. V. & Ribbe, P. H., Quadratic elongation: a quantitative measure of distortion in coordination polyhedra. *Science*, **172** (1971) 567–70.